Cerebral Cortex Advance Access published April 9, 2010

Cerebral Cortex
doi:10.1093/cercor/bhq058

Brain Hemispheric Structural Efficiency and Interconnectivity Rightward Asymmetry in Human and Nonhuman Primates

Yasser Iturria-Medina[1], Alejandro Pérez Fernández[2,3], David M. Morris[4,5], Erick J. Canales-Rodríguez[6,7], Hamied A. Haroon[4,5], Lorna García Pentón[2], Mark Augath[8], Lídice Galán García[1], Nikos Logothetis[4,8], Geoffrey J. M. Parker[4,5] and Lester Melie-García[1]

[1]Neuroimaging Department, Cuban Neuroscience Center, CP 10 600, La Habana, Cuba, [2]Laboratory of Cognitive Neuroscience, Universidad Diego Portales, 8370076 Santiago, Chile, [3]Centro de Investigación y Desarrollo del Comercio Interior, CID-CI, CP 10 400, La Habana, Cuba, [4]Imaging Science and Biomedical Engineering Research Group, School of Cancer and Imaging Sciences and, [5]Imaging Science and Biomedical Engineering, Biomedical Imaging Institute, University of Manchester, Manchester, M13 9PT, UK, [6]Centro de Investigación Biomédica en Red de Salud Mental (CIBERSam), 28007, Madrid, Spain, [7]Benito Menni Complex Assistencial en Salut Mental, Barcelona 08830, Spain and [8]Physiology of Cognitive Processes Department, Max Planck Institute for Biological Cybernetics, 72076 Tübingen, Germany

Address correspondence to Yasser Iturria-Medina, Neuroimaging Department, Cuban Neuroscience Center, Avenida 25, Esquina 158, #15202, Apartado Postal 6648, Cubanacán, Playa, Habana 6 CP 10600, Cuba. Email: iturria.medina@gmail.com.

Evidence for interregional structural asymmetries has been previously reported for brain anatomic regions supporting well-described functional lateralization. Here, we aimed to investigate whether the two brain hemispheres demonstrate dissimilar general structural attributes implying different principles on information flow management. Common left hemisphere/right hemisphere structural network properties are estimated and compared for right-handed healthy human subjects and a nonhuman primate, by means of 3 different diffusion-weighted magnetic resonance imaging fiber tractography algorithms and a graph theory framework. In both the human and the nonhuman primate, the data support the conclusion that, in terms of the graph framework, the right hemisphere is significantly more efficient and interconnected than the left hemisphere, whereas the left hemisphere presents more central or indispensable regions for the whole-brain structural network than the right hemisphere. From our point of view, in terms of functional principles, this pattern could be related with the fact that the left hemisphere has a leading role for highly demanding specific process, such as language and motor actions, which may require dedicated specialized networks, whereas the right hemisphere has a leading role for more general process, such as integration tasks, which may require a more general level of interconnection.

Keywords: brain structural network, diffusion-weighted MRI, efficiency, fiber tractography, hemispheric asymmetries, interconnectivity

Introduction

The interregional structural connectivity asymmetry for left–right brain hemispheres is an important topic in the study of the neural basis of brain functional asymmetries, contributing to our understanding of the factors that modulate cognitive specialization in the brain. The recent development of diffusion–weighted magnetic resonance imaging (DW-MRI), a noninvasive technique that quantifies water diffusion process, has allowed the acquisition of structural information about the intravoxel axon arrangement, making possible the noninvasive study of the brain anatomical circuitry (Mori et al. 1999; Koch et al. 2002; Parker et al. 2002; Behrens, Johansen-Berg, et al. 2003; Tuch et al. 2003; Hagmann, Kurant, et al. 2006; Iturria-Medina et al. 2007). In that context, structural asymmetries have been explored analyzing mainly the fractional anisotropy (FA), a measure of local fiber coherence (Kubicki et al. 2002; Gong et al. 2005; Powell et al. 2006; Clark et al. 2007; Rodrigo et al. 2007) and the number of, or existence of, connecting paths between specific regions (Parker et al. 2005; Hagmann, Cammoun, et al. 2006; Powell et al. 2006; Glasser and Rilling 2008), contributing to our understanding of cognitive lateralized process like language and motor control.

These previous interregional studies were focused on identifying which white matter regions and/or connections, corresponding to reported functional lateralization, are more coherent or stronger in one hemisphere than in the other. In other words, to match well-described functional lateralization with the specific white matter structural asymmetries supporting the function. However, in order to characterize brain structural asymmetry through white matter connections, it is necessary to recognize not only the specific interregional asymmetries in a pairwise manner, which could represent a considerable challenge due to the high number of possible connections, but also the broader structural network asymmetries between the hemispheres, in order to assess differences in how their anatomical substrates may be configured to facilitate the management and integration of information flow in a more general sense.

In this study, we aimed to investigate if, besides the specific regional asymmetries, both hemispheres demonstrate dissimilar general structural attributes implying different principles on the management of the information flow. Our analysis is based on a mathematical network framework (Watts and Strogatz 1998; Latora and Marchiori 2001; Onnela et al. 2005; Boccaletti et al. 2006; Costa et al. 2007), allowing us to explore hemispheric differences in terms of quantitative parameters that can be structurally and, by inference, functionally interpreted. Previous brain structural network analyses have used connectivity information obtained from nonhuman post-mortem studies (Sporns and Zwi 2004; Costa and Sporns 2005; Sporns 2006), statistical concurrent change analysis between brain areas in one or more morphological variables (He et al. 2007; Bassett et al. 2008; Chen et al. 2008; He et al. 2008), or DW-MRI techniques (Hagmann, Kurant, et al. 2006; Hagmann et al. 2008; Iturria-Medina et al. 2008; Gong et al. 2009) to investigate large-scale connection patterns of the brain, such as small-world attributes, efficiency, degree distribution, motif composition, and structural core properties. Here, using 3 different tractography algorithms and a graph theory framework, we attempt to estimate white matter interregional

axonal pathways and to infer left and right common anatomical network properties, obtaining global and local measures that allow us to evaluate for the first time structural network (dis)similarities between hemispheres. In particular, we focus on graph measures of efficiency and interconnectivity, for 11 right-handed healthy human subjects and a single macaque monkey. Additional analyses include the identification of those anatomic regions that are significantly more central or indispensable (in terms of their connections) for the whole-brain structural network than their homolog regions in the opposite hemisphere. Finally, some comments are made concerning the relationship between the obtained anatomical findings and some previously reported functional asymmetries, such as visual attention neglect.

Materials and Methods

Data Acquisition and Preprocessing

Dataset 1

High-angular resolution DW-MRI datasets were acquired in 11 right-handed healthy subjects (age range: 23–38 years). All subjects provided informed consent, and the procedures were approved by the Local Research Ethics Committee. Handedness was determined by documenting the dominant hand of the participants.

Data were acquired on a 3-T Philips Achieva scanner (Philips Medical Systems) in Manchester, UK, using an 8-element SENSE head coil. Diffusion-weighted imaging was performed using a dual phase encoded pulsed gradient spin echo protocol designed to allow correction of susceptibility-induced and eddy current–induced distortions (Embleton et al. 2006). Acquisition parameters used were time echo (TE) = 54 ms, time repetition (TR) = 11884 ms, $G = 62$ mT/m, half-scan factor = 0.679, 112 × 112 image matrix reconstructed to 128 × 128 using zero padding, reconstructed resolution = 1.875 × 1.875 mm^2, slice thickness = 2.1 mm, 60 contiguous slices, 61 noncollinear diffusion sensitization directions at $b = 1200$ s/mm^2 ($\Delta = 29.8$ ms and $\delta = 13.1$ ms), 1 at $b = 0$, and SENSE acceleration factor = 2.5. For each diffusion gradient direction, 2 separate volumes were obtained with opposite polarity *k* space traversal in order to enable the distortion correction method.

T_2-weighted images were also acquired and automatically parcellated into 90 gray matter structures (parcellation scheme 1) (Mazziotta et al. 1995) using the IBASPM toolbox (available at http://www.fil.ion.ucl.ac.uk/spm/ext/#IBASPM) (Alemán-Gómez et al. 2006). Additionally, in order to evaluate possible parcellation scheme effects on lateralization of global/local efficiency and interconnectivity network measures, the registered T_2-weighted images were also parcellated into 71 gray matter structures (parcellation scheme 2) corresponding to the Jacob Atlas developed by the Montreal Neurological Institute (http://www.mni.mcgill.ca/). In order to consider the same left and right gray matter regions, the brain stem region was rejected from this parcellation scheme (for details please see Supplementary Table 4).

Dataset 2

A high-angular resolution DW-MRI dataset was acquired in a formalin-fixed postmortem macaque (*Macaca mulatta*) brain using a Bruker BIOSPEC 4.7-T vertical bore scanner. The macaque brain was perfused, removed from the skull, and kept in 4% paraformaldehyde for 5 years prior scanning. A 2D spin echo MRI sequence was implemented with TE = 78 ms, TR = 9 s, $G = 47$ mT/m, 104 × 94 imaging matrix, 58 contiguous slices, isotropic voxel resolution = 0.8 mm, 61 non-collinear diffusion sensitization directions at $b = 4000$ s/mm^2 ($\Delta = 39$ ms and $\delta = 31$ ms), 7 at $b = 0$, and 4 averages. The total imaging time was ca. 64 h. To improve the signal-to-noise ratio in the diffusion-sensitized images, for the purposes of tractography, we applied 5 iterations of 2D anisotropic diffusion smoothing (rsb.info.nih.gov/ij/plugins/anisotropic-diffusion-2d.html) using ImageJ (rsb.info.nih.gov/ij/index.html).

Following the procedure described in Haroon et al. (2008), we took the cortical parcellation scheme LVE00a (Lewis and Van Essen 2000) available as part of the Caret 5.5 software (available at http://www.brainmap.wustl.edu/caret) for the F99UA1 rhesus macaque brain atlas. Then, using the Normalize tool in SPM5 (available at http://www.fil.ion.ucl.ac.uk/spm/software/spm5/), a nonlinear warping was applied to the F99UA1 MRI brain volume to spatially match the brain volume of our dataset. Finally, the nonlinear warping transformation parameters obtained were applied to the LVE00a parcellation scheme (for a list of region labels see Supplementary Table 5). In addition, macaque cortex structural connections information derived by invasive tracer studies was extracted from Cocomac LVE00a database (cocomac.org/home.asp) (for details please see Fig. 3*a*).

Voxel-Region Axonal Connectivity Estimation

For each subject of datasets 1 and 2, 3 axonal connectivity values between each brain voxel and the surface of each considered gray matter region (voxel-region connectivity) were estimated using 3 fully automated fiber tractography algorithms as follows:

1. Probabilistic tractography from the seed regions was carried out according to Behrens, Woolrich, et al. (2003) using the FSL software package (available at http://www.fmrib.ox.ac.uk/fsl/). For each brain voxel, an index of connectivity, representing the number of generated paths that passed through it from the seed region, was assigned. Tracking parameters used were 5000 as number of generated paths from each seed point (suggested in the FSL software package as optimum to reach the convergence of the algorithm), 0.5 mm as step size, 500 mm maximum trace length, and a curvature threshold of ±80°. In the text we refer to this algorithm as "FSL."
2. Second, probabilistic tractography was performed using the PICo algorithm (Parker et al. 2003; Parker and Alexander 2005). Similarly to the FSL method, a connection probability value with each seed region was assigned to the brain voxels. Tracking parameters used were 5000 as number of generated paths from each seed point, 0.5 mm as step size, 500 mm as maximum trace length, and a curvature threshold over voxel of ±90°. Intravoxel probability density functions of fiber orientation were generated using a model-based residual bootstrap Q-ball approach (Haroon et al. 2009). In the text we refer to this algorithm as "PICo."
3. Finally, a graph-based tractography algorithm (Iturria-Medina et al. 2007) was used, assigning to each brain voxel a probability of connection with each considered seed region. A maximum of 500 mm trace length and a curvature threshold of ±90° were imposed as tracking parameters. The intravoxel white matter orientational distribution function maps were estimated using the Q-ball approach (Tuch 2004). In the text we refer to this algorithm as "GM."

Additionally, in order to evaluate the performance of the previous fiber tractography algorithms (FSL, PICo, and GM) in comparison with the more often used deterministic streamline tractography (SLT) algorithm (Mori et al. 1999), we used also the SLT approach to estimate axonal connectivity values between brain voxels and the surface of each considered gray matter region for the macaque monkey subject (dataset 2). Tracking parameters used for SLT algorithm were 0.5 mm as step size, 500 mm as maximum trace length, a curvature threshold over voxel of ±60°, and a FA threshold of 0.2. Seed points were selected as all brain voxels with an FA value greater than 0.2 (the so-called brute-force approach). Following the procedure described in Li et al. (2009), 2 gray matter regions were considered to be connected if the reconstructed fiber trajectories with 2 end points located in these 2 regions, respectively, were present, and a final connection measurement between these regions was defined as the number of connecting fiber trajectories relative to the number of voxels over the surface of both regions (equivalent to arc weight definition in eq. 1).

Network Construction

For each subject, whole-brain undirected weighted networks were created for each tracking algorithm used as follows: 1) A node was defined to represent each considered anatomic region, 2) An

undirected arc a_{ij} between nodes i and j was established if a nonzero connectivity value was found to exist between the boundary voxels of regions i and j, and 3) Arc weight $w(a_{ij})$ was defined as the connection measurement (the output of the tractography algorithm) between regions i and j (Iturria-Medina et al. 2007), estimated by counting the "effective" number of voxels over the surface of both regions and weighting each voxel by its voxel-region connectivity value with the opposite zone, relative to the total number of considered superficial voxels. Mathematically:

$$w(a_{ij}) \equiv w(a_{ji}) = \frac{\sum_{\forall \vec{r}_n \in N_i^s} \zeta_{\vec{r}_n} + \sum_{\forall \vec{r}_m \in N_j^s} \zeta_{\vec{r}_m}}{\left|N_i^s\right| + \left|N_j^s\right|}, \quad (1)$$

where the term $\zeta_{\vec{r}_n}$ denotes the axonal connectivity value of each node $\vec{r}_n \in N_i^s$ (N_i^s being the set of superficial nodes of region i) with the superficial nodes of region j $\left(N_j^s\right)$. Similarly, $\zeta_{\vec{r}_m}$ denotes the connectivity value of any node $\vec{r}_m \in N_j^s$ with superficial nodes of region i. $\left|N_i^s\right|$ and $\left|N_j^s\right|$ are the number of elements (superficial nodes) of regions i and j, respectively. Note that the first term of the numerator quantifies connections of the region i with j, and the second term quantifies connections of the region j with i.

Eliminating interhemispheric connections, each whole-brain network was segmented into left and right hemispheric networks, each one containing the same number of homolog regions. Graphically, each created undirected weighted network is a discrete set of points (nodes) representing anatomic regions and a set of nondirectional lines (arcs) representing connections between them, which the width of each line reflecting the corresponding arc weight.

Graph Analysis

Efficiency

In terms of the information flow, the global efficiency (E_{glob}) of a network G reflects how efficiently information can be exchanged over G, considering a parallel system in which each node sends information concurrently along the network. It is defined as (Latora and Marchiori 2001):

$$E_{glob} = \frac{1}{n(n-1)} \sum_{\substack{i,j \in G \\ i \neq j}} \frac{1}{d_{ij}}, \quad (2)$$

where n is the number of nodes, and d_{ij} is the geodesic length over all pairs of nodes. In the unweighted network context, the shortest path length d_{ij} is defined as the number of arcs along the shortest path connecting nodes i and j. In the case of weighted networks, the path with the minimum number of nodes is not necessarily the optimal d_{ij} and is necessary to define a physical length associated to each arc (this should be a function of the characteristics of the hypothetical link among any nodes i and j). In this work, we assumed that the physical length of an arc connecting nodes i and j is inversely proportional to the strength of the analyzed connection (Iturria-Medina et al. 2008), i.e., $l_{ij} = \frac{1}{w_{ij}}$. Thus, the shortest path length d_{ij} is finally computed as the smallest sum of the arc lengths throughout all the possible paths from node i to node j. Note that for the particular case of unweighted graphs, $l_{ij} = 1$ for all arcs and the geodesic lengths d_{ij} reduces to the minimum number of arcs traversed to get from i to j.

The local efficiency (E_{loc}) of G is defined as the average efficiency of the local subgraphs (Latora and Marchiori 2001):

$$E_{loc} = \frac{1}{n} \sum_{i \in G} E_{glob}(G_i), \quad (3)$$

where G_i is the subgraph of the first neighbors of node i. This measure has been used to reveal how much a system is fault tolerant, showing how efficient the communication is among the first neighbors of i when i is removed.

In a physiological sense, the global efficiency of a structural brain/hemispheric network reflects the potential parallel exchange of neural information between the involved anatomic regions (a high global efficiency value, i.e., $E_{glob} \approx 1$, may indicate highly parallel information transfer in the brain/hemispheric system, in which each element node could efficiently send information concurrently along the network). The local efficiency of a structural brain/hemispheric network reflects its potential tendency to present communities or clusters of anatomically and physiologically different regions that deal with common neural information (where regions connected to a same region tend also to link to each other). In addition, concurrent higher values of global and local efficiencies indicate a system with a high balance between local necessities (fault tolerance) and wide-scope interactions.

Interconnectivity

In order to obtain a measure of the total amount of connectivity in a weighted network G, here we define the interconnectivity (I_{conn}) of G as the sum of its arc weights. It reflects the amount of connectivity between all the considered anatomic regions.

Betweenness Centrality

Betweenness centrality is a widely used measure to identify the most central nodes in a graph, which are associated to those nodes that act as bridges between the others nodes (Freeman 1977; Bassett et al. 2006; Dall'Asta et al. 2006; Honey et al. 2007). It is defined as the fraction of shortest paths between pairs of nodes that passes through a given node. Mathematically, for weighted networks, if σ_{kj}^w is the number of paths from node k to node j, and $\sigma_{kj}^w(i)$ is the number of these paths passing through node i, the weighted betweenness centrality of i is (Dall'Asta et al. 2006)

$$b_i^w = \sum_{\substack{k,j \in G \\ k \neq j \neq i}} \frac{\sigma_{kj}^w(i)}{\sigma_{kj}^w}. \quad (4)$$

Lateralization Index

In order to characterize asymmetry for a given network measure X (global/local efficiency, interconnectivity, or betweenness centrality), a lateralization index (LI) was computed as:

$$\mathrm{LI}(X) = 100 \times \frac{X(\mathrm{Right}) - X(\mathrm{Left})}{X(\mathrm{Right}) + X(\mathrm{Left})}. \quad (5)$$

This procedure allows us to look at differences between the right and left hemispheres, incorporating the relative network value of X over both hemispheres in one value. The index, ranging between 100 and −100, is positive when X is more prominent over the right hemisphere and lower over the left hemisphere ($X(\mathrm{Right}) > X(\mathrm{Left})$) and negative when the opposite is the case ($X(\mathrm{Right}) < X(\mathrm{Left})$).

Receiver Operating Characteristic Analysis

Receiver operating characteristic (ROC) curves are useful for visualizing, organizing, and selecting classifiers based on their performance (Fawcett 2006). Here, in order to evaluate the performance of the FSL, PICo, and GM fiber tractography algorithms in comparison with the traditional SLT algorithm, ROC curves for each of these algorithms were constructed, based on the comparison of their connection results for the macaque monkey subject (dataset 2) and the reference connection pattern defined by macaque cortex structural connections information derived by invasive tracer studies (Fig. 3*a*).

First, because in this analysis we are not differencing between left and right hemispheres due to connection information from invasive tracing studies not being hemisphere specific, connectivity matrix representing each fiber tractography algorithm was created assuming, as final connection value between any 2 regions i and j, the mean of the connection values obtained by this algorithm on both hemispheres (eq. 1). Next, the ROC curve corresponding to a specific tractography algorithm was represented as the fraction of "true positives" (TPR) versus the fraction of "false positives" (FPR) of its connectivity matrix with regard the reference connection pattern (Fig. 3*a*) as a discrimination threshold is varied, that is, a set of threshold values, varying from minimum to maximum value, were applied to the analyzed connectivity matrix and resulting binarized matrix versions were compared with

the reference connection pattern (Fig. 3*a*), allowing to calculate corresponding TPR and FPR values as:

$$\mathrm{TPR} = \frac{\mathrm{TP}}{\mathrm{TP} + \mathrm{FN}}, \qquad \mathrm{FPR} = \frac{\mathrm{FP}}{\mathrm{FP} + \mathrm{TN}}, \tag{6}$$

where TP, FN, FP, and TN are the number of true positives, false negatives, false positives, and true negatives, respectively. For a valid comparison, only those matrix cells where a direct (dis)connection by invasive tracer studies (values 0 and 1 on Fig. 3*a*, i.e., a total of 462 values) have been reported were considered. One point in ROC space is considered better than another (each point belonging to a different tracking algorithm) if it is to the northwest (TPR is higher, FPR is lower, or both).

Results

Anatomical connections between cortical and subcortical regions for 11 right-handed healthy human subjects (dataset 1) and a single macaque monkey (dataset 2) were estimated using 3 different fiber tractography algorithms (see Materials and Methods). From the obtained voxel-region connectivity maps (Fig. 1*b*), weighted networks were created for the whole brain (Fig. 1*c*), in which each node represents an anatomic brain region (90 for humans or 176 for macaque monkey), arcs connecting nodes correspond to white matter links, and arc weights correspond to the degree of evidence supporting the

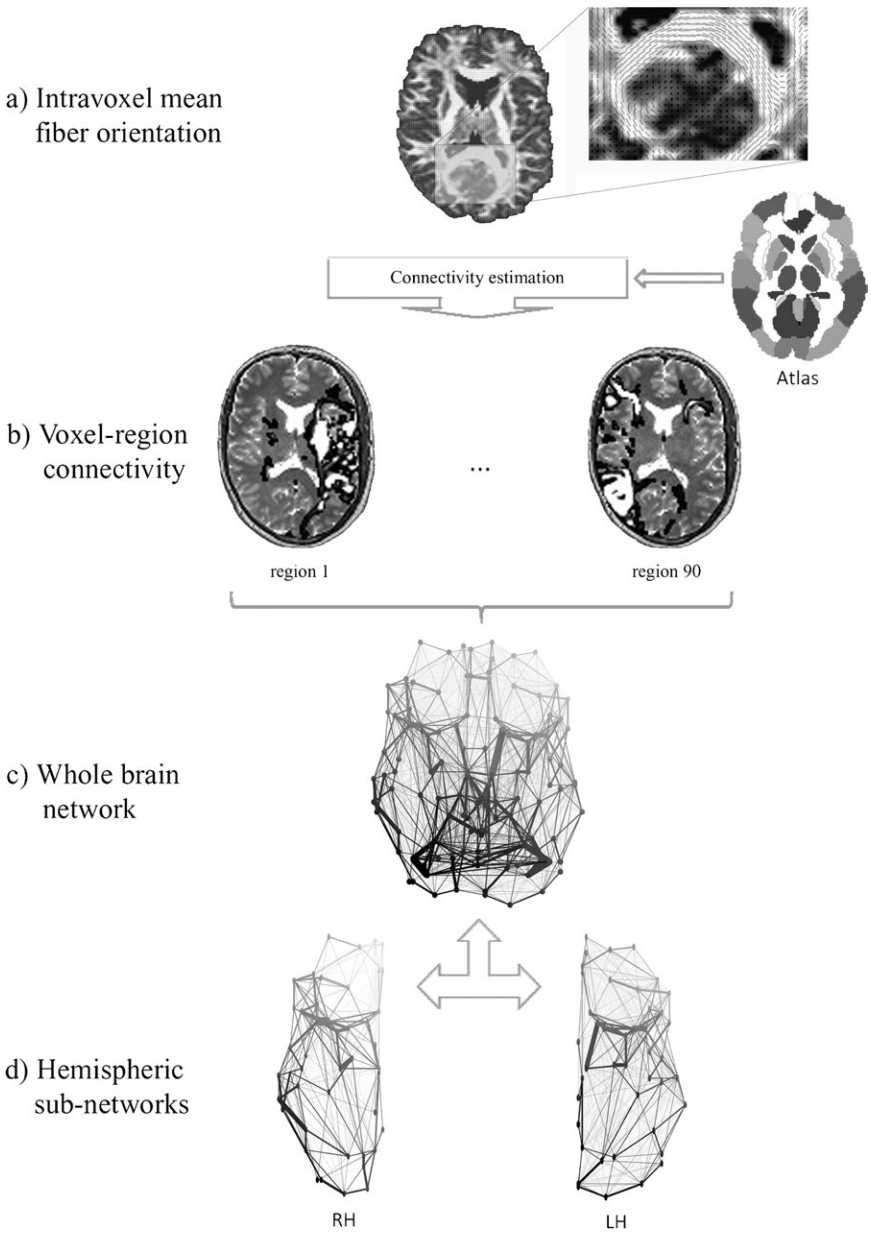

Figure 1. Schematic representation of the connectivity estimation and network construction procedure; for an example, human subject and the first tractography algorithm. (*a*) Axial map representing intravoxel mean fiber orientation (dyadic vectors), overlaid on the FA image; the inset figure provides detail of the high fiber orientation coherence within the splenium of the corpus callosum. (*b*) Axial voxel-region connectivity maps corresponding to region 1 (precentral gyrus) and region 90 (inferior temporal gyrus), overlaid on the registered T_2-weighted image; voxels are color-coded according to whether the connectivity of each voxel is high (white) or low (black). (*c*) Whole-brain structural network derived as described in Materials and Methods. (*d*) Right and left hemispheric networks (RH and LH, respectively), obtained by rejection of callosal connections on the whole-brain structural network (viewed from below). In (*c*) and (*d*), points (nodes) represent anatomic regions, lines without arrow (arcs) correspond to connections between them, and line widths reflect the corresponding arc weights. Lines colors were assigned according to the spatial position of the nodes.

existence of a white matter connection between regions. Eliminating callosal connections, each whole-brain network was segmented into left and right hemispheric networks, each one containing the same number of homolog regions (i.e., 45 regions for humans and 88 regions for macaque monkey; Fig. 1*d*).

In summary, for each subject we obtained a whole-brain network, and corresponding left/right hemispheric networks, each one replicated for each of 3 different fiber tracking algorithms.

Efficiency and Interconnectivity Asymmetries

We evaluated structural asymmetries between left hemisphere and right hemisphere networks according to 3 network properties: global efficiency (E_{glob}, a measure of how efficiently information can be exchanged over a network), local efficiency (E_{loc}, the average global efficiency of the local subnetworks), and interconnectivity (I_{conn}, a measure of the total amount of interconnectivity). These measures were separately computed for each individual's left and right hemispheric networks (see Materials and Methods).

In order to characterize the hemispheric asymmetry for global/local efficiency and interconnectivity, a LI was calculated for each of these 3 network measures, with a positive value meaning a lateralization to the right while negative value indicates a lateralization to the left (see Materials and Methods). Interestingly, the obtained LI results showed a consistent lateralization trend toward the right hemisphere for the 3 efficiency and interconnectivity network measures (Fig. 2).

Before testing for a statistically significant lateralization for human subjects, we compared tracking algorithm effects on the obtained LI values using a Kruskal–Wallis test, testing the null hypothesis that all values for a same network measure (E_{glob}, E_{loc}, or I_{conn}) were drawn from the same distribution independently of the fiber tracking algorithm used. The nonsignificant P values obtained ($P > 0.05$; Table 1) supported that LI values obtained were not statistically dependent on the tracking method used. Right lateralization was then tested using a sign test with the hypothesis that all obtained LI values for a same network measure come from a distribution whose median is zero. The small P values obtained (all $P < 7 \times 10^{-5}$; Table 1) supported the hypothesis of a significant positive lateralization for the 3 measures, indicating that human right hemisphere networks are anatomically more efficient and interconnected than left hemisphere networks for right-handed subjects. The LI values obtained for E_{glob}, E_{loc}, and I_{conn} in the macaque monkey were also positive for the 3 tractography algorithms (Table 1).

Regional Betweenness Centrality Asymmetries

We computed the betweenness centrality associated with each brain region considered in humans (dataset 1) and macaque monkey (dataset 2) with respect to the whole-brain anatomical network. This measure reflects the relative centrality or indispensability of each gray matter region within the entire brain anatomical network in terms of its connections, in which higher betweenness centrality values imply greater importance (see Materials and Methods). Then, in order to characterize centrality asymmetries between left and right homolog regions, a betweenness centrality LI was calculated (a positive value meaning a lateralization to the right while a negative value indicates a lateralization to the left).

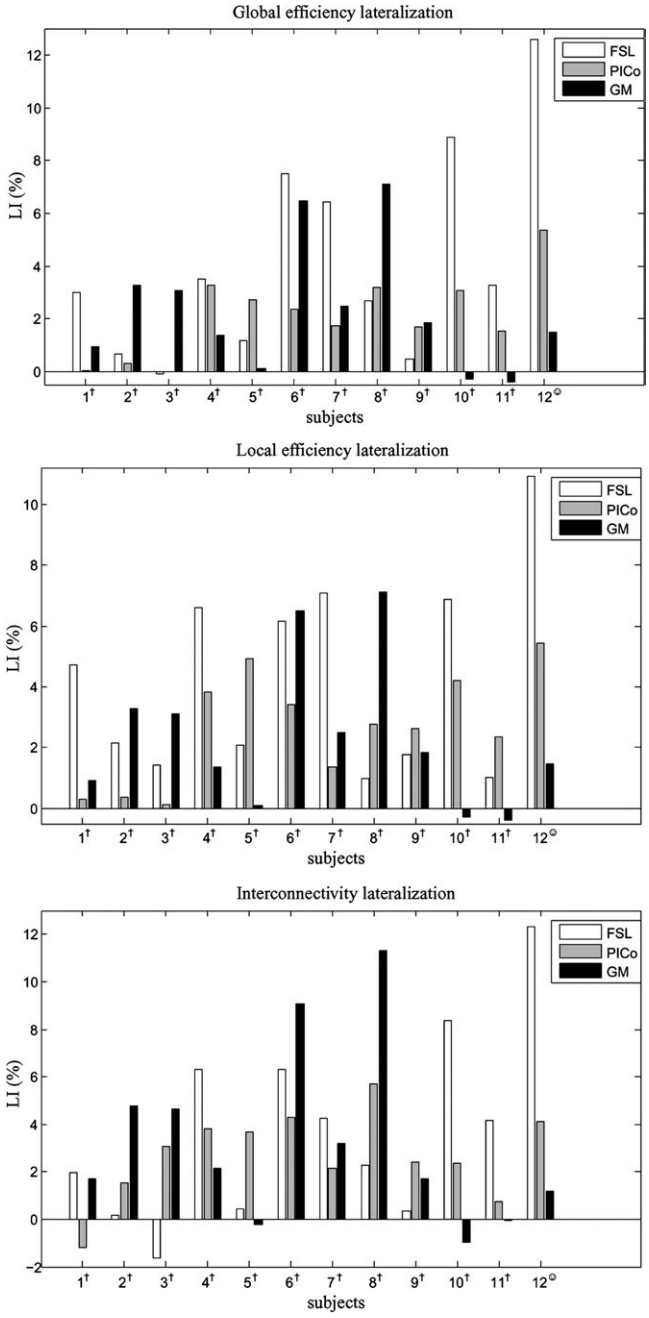

Figure 2. Efficiency and interconnectivity LIs obtained using 3 different fiber tractography algorithms (FSL, PICo, and GM; see Materials and Methods) for 11 right-handed healthy human subjects (dataset 1; denoted by superscript "†") and a nonhuman primate (dataset 2; denoted by superscript "☺"). Each compared left and right hemispheric networks contained the same number of anatomic homolog regions (i.e., 45 for humans or 88 for the nonhuman primate). Note a prevalence of positive bar values, indicating a consistent lateralization to the right hemisphere.

Results in Dataset 1

Before testing for a statistically significant lateralization of the betweenness centrality parameter between human homolog regions, we compared tracking algorithm effects on the measured betweenness centrality LI values using a Kruskal–Wallis test (Table 2). We observed that 9 region pairs had betweenness centrality values that were dependent on method but that the remaining 36 region pairs did not ($P > 0.05$). In a first lateralization analysis, we considered only those 36 pairs

Table 1

Global efficiency, local efficiency, and interconnectivity LIs obtained for the brain anatomical networks of a single macaque monkey (dataset 2) and 11 right-handed healthy subjects (dataset 1)

Brain networks	Measure	Lateralization (mean ± standard error of the mean)			Kruskal–Wallis (*P*)	Sign test (*P*)
		FSL	PICo	GM		
Macaque	E_{glob}	12.67	5.36	1.48	—	—
	E_{loc}	10.97	5.43	1.48	—	—
	I_{conn}	12.35	4.10	1.18	—	—
Human	E_{glob}	3.39 ± 0.90	1.80 ± 0.37	2.35 ± 0.76	0.4903	$\mathbf{1.09 \times 10^{-5}}$
	E_{loc}	3.71 ± 0.77	2.39 ± 0.50	2.37 ± 0.76	0.4140	$\mathbf{1.30 \times 10^{-7}}$
	I_{conn}	2.98 ± 0.94	2.60 ± 0.56	3.39 ± 1.16	0.9990	$\mathbf{6.61 \times 10^{-5}}$

Note: A positive value means a lateralization to the right hemisphere while a negative value indicates a lateralization to the left hemisphere. For human cases, mean values are reported with their corresponding standard errors (i.e., the uncertainty of how the sample mean represents the underlying population mean). The Kruskal–Wallis *P* values corresponds to the null hypothesis that all human LI values for a given measure (E_{glob}, E_{loc}, or I_{conn}) were drawn from the same distribution independently of the used fiber tracking algorithms. The nonsignificant *P* values obtained (all $P > 0.4$) demonstrates that each tracking method yields statistically indistinguishable results. The sign test *P* value corresponds to the null hypothesis that all the human LI values come from a distribution whose median is zero. The small *P* values obtained (all $P < 7 \times 10^{-5}$) supported the hypothesis of a significant positive lateralization for the 3 measures. For an equivalent statistical analysis, in which the same network measures were directly compared without the use of a LI, please see Supplementary Table 1. Significant values are depicted in bold type.

Table 2

Human considered brain regions (dataset 1, parcellation scheme 1) and corresponding statistical results for obtained betweenness centrality LI values

Region		Kruskal–Wallis (*P*)	Sign test (*P*)	Region		Kruskal–Wallis (*P*)	Sign test (*P*)
No.	Name			No.	Name		
1	**Precentral**	0.3753	**−0.0350**	24	Lingual	0.3974	+1
2	Frontal_Sup	0.3281	+1	25	**Occipital_Sup**	**0.1061**	**+0.0350**
3	Frontal_Sup_Orb	0.7893	+0.4582	26	**Occipital_Mid**	0.0031	**+0.0046**
4	Frontal_Mid	0.7311	−0.0614	27	**Occipital_Inf**	0.4269	**−0.0266**
5	**Frontal_Mid_Orb**	0.1131	**−0.0214**	28	Fusiform	0.1493	−0.4868
6	Frontal_Inf_Oper	0.4402	+1	29	Postcentral	0.5276	−0.3770
7	Frontal_Inf_Tri	0.2545	−0.8600	30	Parietal_Sup	0.6837	−0.1496
8	Frontal_Inf_Orb	0.3326	+0.1686	31	**Parietal_Inf**	$\mathbf{5.34 \times 10^{-5}}$	**−0.0071**
9	Rolandic_Oper	0.3974	+1	32	**SupraMarginal**	0.8089	**+0.0013**
10	**Supp_Motor_Area**	0.5851	**−0.0427**	33	**Angular**	0.2948	$\mathbf{+6.61 \times 10^{-5}}$
11	**Olfactory**	0.2917	**−0.0045**	34	Precuneus	0.4045	+0.0801
12	**Frontal_Sup_Medial**	0.0851	**−0.0059**	35	**Paracentral_Lobule**	0.3069	**−0.0002**
13	Frontal_Mid_Orb	0.0958	+0.2153	36	**Caudate**	0.2482	**−0.0013**
14	Rectus	0.0923	+0.4868	37	Putamen	**0.0059**	+0.2862
15	Insula	0.6338	+0.4868	38	Pallidum	0.2943	+0.5078
16	**Cingulate_Ant**	0.2344	$\mathbf{-1.30 \times 10^{-7}}$	39	Thalamus	0.2421	+0.5966
17	**Cingulate_Mid**	0.4021	**−0.0045**	40	Heschl	$\mathbf{8.52 \times 10^{-6}}$	−1
18	**Cingulate_Post**	**0.0479**	**−0.0043**	41	**Temporal_Sup**	**0.0069**	$\mathbf{-1.09 \times 10^{-5}}$
19	**Hippocampus**	0.5706	**+0.0350**	42	**Temporal_Pole_Sup**	**0.0238**	**−0.0008**
20	ParaHippocampal	0.4523	+0.2004	43	Temporal_Mid	0.2129	+0.8600
21	Amygdala	**0.0030**	+0.1338	44	Temporal_Pole_Mid	**0.0035**	−0.0063
22	Calcarine	0.1609	−1	45	Temporal_Inf	0.0724	−0.8600
23	**Cuneus**	0.4084	**+0.0013**				

Note: The Kruskal–Wallis *P* value corresponds to the null hypothesis that all betweenness centrality LI values for a given region were drawn from the same distribution independently of the used fiber tracking algorithms (a *P* value near to zero, i.e., $P < 0.05$, suggests that at least one sample median is significantly different from the others). The sign test *P* value (preceded by − or + symbols, which indicates a leftward or rightward lateralization, respectively) corresponds to the null hypothesis that the betweenness centrality LI values come from a distribution whose median is zero (a *P* value near to zero, i.e., $P < 0.05$, indicates a significant lateralization). For obtained betweenness centrality LI values corresponding to each region and fiber tracking method, including the complete statistic results of tracking algorithm effects, please see Supplementary Table 2. For an equivalent lateralization statistical analysis, in which the obtained betweenness centrality left/right values were directly compared without the use of a LI, please see Supplementary Table 3. Significant values are depicted in bold type.

of regions whose LI values can be statistically assumed to be drawn from the same distribution for the 3 tracking algorithms. Lateralization was then tested using a sign test, with the hypothesis that all measured LI values of each identified pair of regions came from a distribution whose median is zero.

Significant lateralization of betweenness centrality was found for 15 pairs of homolog regions ($P < 0.05$; Table 2). Leftward asymmetries (negative LI) were observed in 10 pairs of regions: precentral gyrus ($P = 0.0350$), middle orbital frontal ($P = 0.0214$), supplementary motor area ($P = 0.0427$), olfactory bulb ($P = 0.0045$), superior medial frontal gyrus ($P = 0.0059$), anterior cingulate gyrus ($P = 1.30 \times 10^{-7}$), middle cingulate gyrus ($P = 0.0045$), inferior occipital ($P = 0.0266$), paracentral lobule ($P = 0.0002$), and caudate ($P = 0.0013$). Significant rightward asymmetries (positive LI) were observed in 5 pairs of regions: hippocampus ($P = 0.0350$), cuneus ($P = 0.0013$), superior occipital ($P = 0.0350$), supramarginal ($P = 0.0013$), and angular ($P = 6.61 \times 10^{-5}$).

In order to account to a degree for the demonstrated differences in output from different tracking processes, we also assessed those pairs of regions whose LI values can be statistically assumed to be drawn from the same distribution for 2 of the 3 tracking algorithms. Eight additional pairs of homolog regions were included in the lateralization analysis when using this criterion. By means of a sign test, 6 of the additional region pairs were found to demonstrate significant lateralization ($P < 0.05$; Table 2). Leftward (negative LI) asymmetries were observed in posterior cingulate gyrus ($P = 0.0043$), inferior parietal ($P = 0.0071$), superior temporal ($P = 0.0015$), superior temporal pole ($P = 1.09 \times 10^{-5}$), and middle temporal pole (P = 0.0008),

whereas only the middle occipital ($P = 0.0046$) was found to demonstrate rightward asymmetry.

In summary, a total of 21 pairs of human homolog regions were found lateralized in terms of their centrality or indispensability to the whole-brain structural network. In line with a previous cortical thickness study (Luders et al. 2006), we found a more pronounced leftward than rightward asymmetry (15 vs. 6 lateralized regions, respectively).

Results in Dataset 2

Tracking algorithm effects for the macaque monkey data were compared using a Kruskal–Wallis test across all considered region pairs. The high P value obtained ($P = 0.8393$) supported the conclusion that LI values obtained were not statistically dependent on the tracking method used. Lateralization was then tested via a nonparametric permutation test (see Appendix).

Significant lateralization of betweenness centrality was found for 19 pairs of homolog regions ($P < 0.05$). Leftward asymmetry (negative LI) was observed in 11 regions: temporoparietal area ($P = 0.0156$), somatosensory area 2 ($P = 0.0156$), middle temporal area ($P = 0.0313$), ventral subdivisions of the anterior inferotemporal cortex area TE ($P = 0.0156$), dorsal prelunate area ($P = 0.0313$), subdivisions of area 8 ($P = 0.0156$), dorsal cingulate area 24 ($P = 0.0156$), subdivisions of cingulate area 24 ($P = 0.0156$), area 31 ($P = 0.0156$), area 14r ($P = 0.0156$), and medial area 10 ($P = 0.0313$). Significant rightward asymmetry (positive LI) was observed in 8 regions: visual area 3 ($P = 0.0156$), visual area V3A ($P = 0.0156$), area 13m ($P = 0.0156$), ventral visual area ($P = 0.0156$), 11m ($P = 0.0156$), medial intraparietal area ($P = 0.0313$), area 6M ($P = 0.0156$), and area 32 ($P = 0.0156$).

Fiber Tracking Algorithms Performance Evaluation

In order to evaluate the validity of the fiber tractography algorithms used in this paper (FSL, PICo, and GM) in comparison with the more often used deterministic SLT algorithm (Mori et al. 1999), we compared structural networks results obtained for the macaque monkey (dataset 2) with macaque cortex structural connections information derived by invasive tracer studies. Figure 3*a* presents cortical–cortical connection information extracted from Cocomac LVE00a database, corresponding to 63 brain cortical regions (see Materials and Methods, Data Acquisition and Preprocessing), whereas Figure 3*b* presents resultant ROC curves from comparison between previous cortical–cortical connection information and connectivity matrices estimated with FSL, PICo, GM, and SLT algorithms (see Materials and Methods, Receiver Operating Characteristic Analysis).

Although it is not possible to make a statistical comparison between the obtained ROC curves (due to the fact that they correspond to a single dataset), a clear prevalence of the 3 fiber tracking algorithms used in this study (FSL, PICo, and GM) can be seen over the performance of the traditional deterministic SLT algorithm, which is also numerically supported by the corresponding areas under the ROC curves: FSL (AUC = 0.78), PICo (AUC = 0.72), GM (AUC = 0.77), and SLT (AUC = 0.62).

Discussion

We performed a structural network analysis based on DW-MRI techniques and graph theory to identify brain hemispheric anatomical asymmetries. In contrast with previous structural network studies (Hagmann, Kurant, et al. 2006; Hagmann et al. 2008; Iturria-Medina et al. 2008; Gong et al. 2009), here we

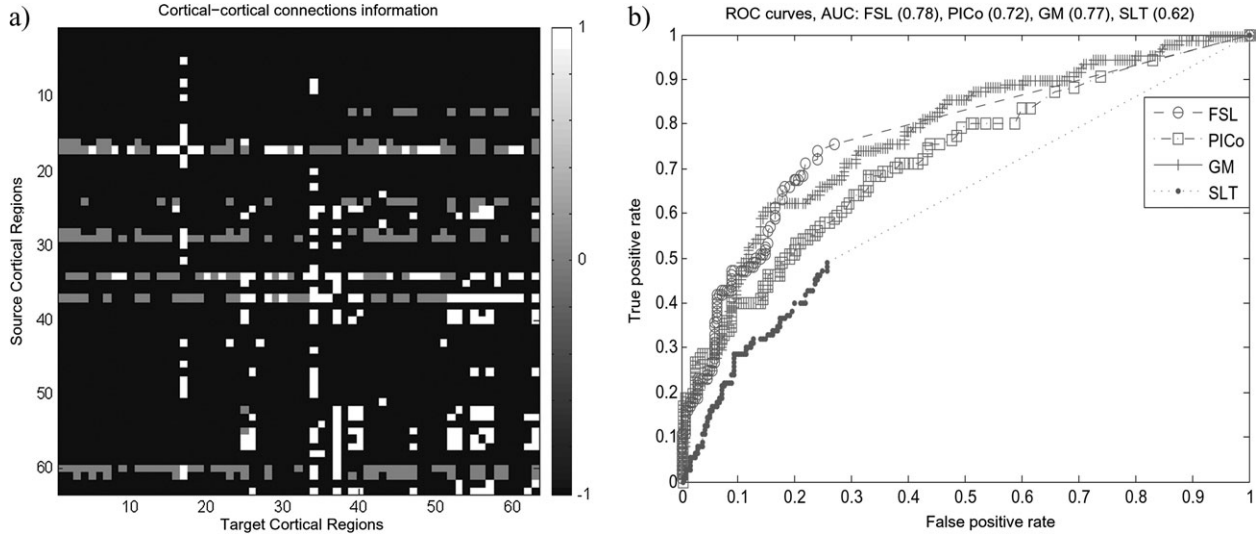

Figure 3. Macaque cortex structural connections derived by invasive tracer studies and ROC curves resulting from a comparison with connections derived by DW-MRI tractography techniques. (*a*) Cortical–cortical connection information extracted from Cocomac LVE00a database (cocomac.org/home.asp). Similarly to methods in Haroon et al. (2008), the source and target cortical regions, numbered 1 to 63 on the matrices, correspond to the subset of cortical areas labeled as follows in the LVE00a scheme: 1, 2, 4, 23, 45, 24d, 3a, 46p, 46v, 4C, 5D, 5V, 6Ds, 6Val, 6Vam, 7a, 7b, 7op, 7t, 8Ac, 8Am, 8As, A1, AIP, DP, FST, G, IPa, LIPd, LIPv, LOP, MDP, MIP, MSTda, MSTdp, MSTm, MT, Pi, PIP, PO, PrCO, Ri, S2, TAa, TE1–3, TEa/m, TF, TPOc, TPOi, TPOr, Tpt, V1, V2, V2v, V3, V3A, V4, V4ta, V4tp, VIPl, VIPm, VOT, and VP, respectively. Values of 1 (or 0) have used to fill in cells where there is (or not) a direct connection, while a value of −1 has been used for connections for which no information is available. (*b*) Resultant ROC curves from comparison between previous cortical–cortical connection information and connectivity matrices estimated with FSL, PICo, GM, and traditional SLT (Mori et al. 1999) algorithms, for a single macaque monkey (dataset 2). For a valid comparison, we considered only those matrix cells where have been reported a direct (dis)connection by invasive tracer studies (values 0 and 1 on panel *a*). Although it is not possible to make a statistical comparison between the obtained ROC curves (due to the fact that they correspond to a single dataset), a clear prevalence of the 3 probabilistic fiber tracking algorithms used in the study (FSL, PICo, and GM) can be seen over the performance of the traditional deterministic SLT algorithm, which is also numerically supported by the corresponding areas under the ROC curves: FSL (AUC = 0.78), PICo (AUC = 0.72), GM (AUC = 0.77), and SLT (AUC = 0.62).

emphasize the use of 3 tractography algorithms, making the results robust to choice of tracking algorithm, which is potentially a significant source of bias, and thus providing a valuable assessment of the relative detail of network information across these methods and, more importantly, providing a robust set of results with which to assess lateralization. We found significant differences between right and left hemispheric networks at a hemispheric level using the metrics E_{glob}, E_{loc}, and I_{conn}, indicating that the right hemisphere is, at the whole-hemisphere level, more efficient and interconnected. However, the subhemisphere regional asymmetries observed using the betweenness centrality measure indicate that the left hemisphere presents more central or indispensable regions for the whole-brain structural network than the right hemisphere. These findings were found to hold true across the human dataset and in the single macaque dataset, indicating that general organizational strategies are broadly similar between these species.

Efficiency and Interconnectivity Hemispheric Asymmetries

We explored general structural differences between both hemispheres via 3 network measures: global efficiency, local efficiency, and interconnectivity (E_{glob}, E_{loc}, and I_{conn}, respectively). A significant rightward asymmetry on both efficiencies and interconnectivity was found (Table 1 and Fig. 2). To our knowledge, this is the first report of brain structural asymmetry of these measures. This whole-hemisphere right-greater-than-left interconnectivity and efficiency are consistent with the reported significant rightward asymmetry in the white matter volume for right-handed healthy subjects (Barrick et al. 2005). Furthermore, the greater efficiency and stronger interconnectivity in the right hemisphere obtained for the macaque monkey suggest that these asymmetry characteristics could be shared among primates, even when caution is applied when considering that a single nonhuman primate case was tested.

Our results raise a number of intriguing questions. For example, what are the functional requirements underlying the fact that one hemisphere is more efficient and interconnected than the other? Interestingly, our leftward regional asymmetry findings, as expressed using the betweenness centrality measure, indicate that left hemisphere presents more central or indispensable regions for the whole-brain structural network than the right hemisphere, which is in line with previous studies (Luders et al. 2006). Since the connectivity of a given region, and thus the measurement of betweenness centrality, is related to its cellular characteristics such as cell packing density, cell size, and number of cortical neurons (Costa 2005; Lerch et al. 2006), connectivity asymmetries of the cortex might be related to hemisphere-specific functional specializations, which based on the high correspondence between our structural results and well-known functional regional asymmetries seems to support the fact that the left hemisphere is "regionally" more specialized than the right hemisphere. When considered in combination with the whole-hemisphere efficiency and interconnectivity results, this induces us to think that a greater left hemisphere functional specialization could lead to its apparently "worse" general structural organization (less efficiency and interconnectivity at the whole-hemisphere scale) in comparison with the right hemisphere. In terms of functional principles, these patterns appear to support the fact that the left hemisphere has a leading role for highly demanding specific process, such as language and motor actions, which may require dedicated specialized networks, whereas the right hemisphere has a leading role for more general process, such as integration tasks, which may require a more general level of interconnection.

Regional Betweenness Centrality Asymmetries, Correspondence with Previous Findings

Previous studies reporting structural differences between homologs areas have been mainly based on specific cytoarchitectonic and morphologic features while our regional asymmetry analysis is based on the fiber connectivity pattern of each region in terms of its relative importance to the whole-brain structural network. Despite the interpretative differences between the measures and procedures employed in different studies, we found a considerable regional correspondence between previous reports, old observations of asymmetric regional specialization (based on the effects of brain lesions), and our asymmetry findings, supporting the hypothesis of a determinant relation between cytoarchitectonic/morphologic characteristics and interregional connectivity (Costa 2005; Lerch et al. 2006; Van Essen 1997).

Dataset 1

In correspondence with previous human studies, leftward asymmetries for the precentral gyrus and supplementary motor area, regions associated with motor control actions as hand preferences, have been well recognized for right-handed subjects (Amunts et al. 1996; Rogers et al. 2004; Dadda et al. 2006; Luders et al. 2006). The paracentral gyrus and cingulate gyrus leftward asymmetries found here are in line with similar cortical thickness results (Luders et al. 2006), although this cingulate gyrus asymmetry is in contrast to rightward asymmetries previously reported using volumetric and voxel-based measures (Paus et al. 1996; Watkins et al. 2001). However, significant left-greater-than-right FA values have previously been reported for the cingulum bundle (i.e., white matter fibers projecting from the cingulate gyrus to the entorhinal cortex), suggesting a more coherent fiber organization in the left hemisphere that is consistent with our findings (Gong et al. 2005; Clark et al. 2007). In addition, our observed leftward asymmetries for superior temporal, superior temporal pole, and middle temporal pole regions agree with many structural reports (Niznikiewicz et al. 2000; Good et al. 2001a; Watkins et al. 2001; Luders et al. 2006) and the documented left hemispheric dominance for language (Price 2000). Nevertheless, we did not find significant localized asymmetries related to the inferior frontal regions, thought to contain Broca's region, which is also associated with dominant language process. Interestingly, a recent study (Keller et al. 2009) concluded that contrary to what has frequently been reported in literature, structural asymmetry of Broca's area has not been reproducibly demonstrated. According to this previous study, if a structural asymmetry of Broca's area does exist, it is variable and may differ from that of the functional asymmetry of language, which is more consistent. Additionally, it is known that the gyral location and extent of Broca's area vary considerably between subjects (Amunts et al. 1999, 2004; Mazziotta et al. 2001; Juch et al. 2005; Lindenberg et al. 2007). Such variation has been demonstrated using cytoarchitectonic and functional imaging methods but cannot be determined

from the purely anatomical parcellation of the cortex used in our study. We must therefore conclude that there is a possibility that a true underlying localized lateralization associated with Broca's area has not been detected using our methodology.

Asymmetries of the caudate nucleus, a region found here with a leftward betweenness centrality asymmetry and thought to be involved in higher order motor control (Graybiel 2005) and learning and memory process (Packard and Knowlton 2002), have been reported for normal children (Filipek et al. 1997; Pueyo et al. 2000; Castellanos et al. 2001) and for children with attention-deficit hyperactivity disorder (Aylward et al. 1996; Sugama et al. 2000; Castellanos et al. 2001; Schrimsher et al. 2002). However, reports on caudate asymmetry have been inconsistent (e.g., in normal subjects a common finding is left-greater-than-right caudate volume although there are also reports of no asymmetry and even of rightward asymmetry; see Schrimsher et al. 2002). Recently, Tremols et al. (2008) argued that these inconsistencies can be explained according to different asymmetric properties of the head and body parts of the caudate, which connect into different fiber pathways. Unfortunately, our study was limited to the whole caudate region without making distinction between its head and body parts due to the nonspecificity of our gray matter parcellation scheme. Further caudate network analysis should focus on more precise parcellations in order to explore how caudate connectivity could be related to head and body volume asymmetries.

In the case of those homotopic regions found with a betweenness centrality rightward asymmetry, the finding of the hippocampus is consistent with the widely reported right-sided asymmetries for this region (Free et al. 1995; Bigler et al. 1997; Bilir et al. 1998; Good et al. 2001b; Pegues et al. 2003). It is striking that all the other right-lateralized regions (i.e., cuneus, superior occipital, supramarginal, angular, and middle occipital) are related to visual processes, and there is evidence that right hemispheric areas play a dominant role in the implementation of visuo-spatial attention (Fink et al. 2000, 2001; Corbetta and Shulman 2002; Halligan et al. 2003). The specific case of a betweenness centrality rightward lateralization for angular and supramarginal gyrus (Brodmann areas 39 and 40, respectively) is an additionally interesting result because evidence exists suggesting that lesions to these regions on the right hemisphere cause visuo-spatial attentional neglect (Vallar 1998; Halligan et al. 2003; Husain and Rorden 2003), a neuropsychological syndrome characterized by an attentional bias. To our knowledge, this is the first structural indication of why the widely investigated phenomenon of visuo-attentional neglect is more commonly a consequence of right hemisphere damage.

Dataset 2

Literature about macaque monkey interhemispheric brain asymmetries is scarce. However, in correspondence with our results, consistent evidence concerning leftward volumetric asymmetry at the cytoarchitectural level of the temporoparietal area (Tpt) has been reported (Gannon et al. 2008). This region, a homologous area of the human planum temporale, is thought to be linked to the participation of the left temporal lobe in auditory and vocalization process, cognitive tasks that have being reported to present a leftward lateralization in the macaque monkey (Heffner HE and Heffner RS 1984; Poremba et al. 2004). In addition, we found a leftward asymmetry to the middle temporal and the ventral subdivisions of the anterior inferotemporal cortex area TE. These results reinforce the view that the macaque could provide a model system for studying the evolutionary development of concepts and language in humans (Gil-Da-Costa et al. 2004).

Interestingly, we also find corresponding interspecies structural asymmetries in the visual system (rightward asymmetry) and cingulate gyrus (leftward asymmetry), which to our knowledge have not been reported before. However, as the parcellation schemes that we used for human and nonhuman primate differed considerably, further analyses are necessary to identify with confidence other possible asymmetry equivalences and differences between species.

Methodological Issues and Future Work

Previous structural and functional studies have provided evidence on how the apparent topological organization of brain networks can be modified by the different parcellation strategies applied (Hagmann, Kurant, et al. 2006; Li et al. 2009; Wang et al. 2009). In principle, our results could be biased by the chosen gray matter parcellation scheme, a key element of the creation of brain anatomical networks due to its influence on the node definition process. Thus, in order to explore possible parcellation effects on our efficiency and interconnectivity findings, we repeated the human structural brain graph asymmetry analysis for another parcellation scheme with a different set of 70 regions, using 1 of the 3 tractography algorithms (GM), and the results indicated a consistent hemispheric rightward asymmetry on these measures (see Supplementary Figure 1 and Supplementary Table 4). However, it is important to consider that although the atlases that we used were carefully created taking into account relevant anatomical and functional details, in the future it might be more meaningful to use advanced integrative atlases based on finer cytoarchitecture, myeloarchitecture, and MRI procedures (Toga et al. 2006).

In contrast to the more often used deterministic tractography approach (Conturo et al. 1999; Mori et al. 1999; Basser et al. 2000), which typically can only progress when there is high certainty of fiber direction limiting their usefulness in defining pathways near gray matter, the 3 different tractography algorithms used in this study include in the tracking procedure the uncertainty of each fiber orientation (based in the high information contained in the acquired high–angular resolution DW-MRI datasets) and attempt to establish the spatially distributed degree of connection confidence across the whole brain to a given start point. However, in spite its advantages over the conventional deterministic tractography (Fig. 3*b*), these methods still present important limitations, like a decrease in probability of connection with distance and the difficulty to separate real from false connections. Thus, in the future it might be more meaningful to use statistical methodologies such as that recently introduced by Morris et al. (2008), which proposed to address the mentioned limitations of current probabilistic tractography algorithms using an objective method for determining significant connections based on statistical comparison with a null pattern of connection, which also has the desirable effect of reducing the effect of distance on extracted patterns of connection.

Another consideration for our study is the relatively small size of the used subject sample, especially with respect to the

macaque brain. Despite this, as previously mentioned, the use of 3 different tractography algorithms allowed us to replicate network measures, making the statistical analysis nonspecific to only one tracking algorithm's results and thus improving the robustness of the study. However, future work should be addressed to analyzing a bigger number of subjects, taking into account also handedness and sex effects, not considered here in spite their evidenced influence on structural and functional asymmetries.

Supplementary Material

Supplementary material can be found at: http://www.cercor.oxfordjournals.org/

Funding

Biotechnology and Biological Sciences Research Council of the United Kingdom (BB/E002226/1).

Notes

We are also grateful to the anonymous reviewers for their useful comments and suggestions. Author contributions: Y.I.-M. and A.P.F. conceived and designed the experiment. G.J.M.P., D.M.M., H.A.H., M.A., and N.L. acquired and preprocessed the MRI datasets. D.M.M., H.A.H., and G.J.M.P. implemented the PICo tractography algorithm used. Y.I.-M. implemented the graph-based tractography algorithm and network analysis tools used. Y.I.-M. and A.P.F. analyzed the data and wrote the paper with input from all other authors. All authors contributed to constructive discussions regarding the interpretation of the results. C*onflict of Interest*: None declared.

Appendix

Permutation Test Used for the Betweenness Centrality Lateralization Analysis of Dataset 2

The analysis consisted of the following steps (Blair and Karniski 1993; Galan et al. 1997):

1. The null hypothesis (H_0) of 0 mean for all the measured LI values is decomposed into the marginal hypotheses H_{0r}: $m_r = 0$, where m_r is the mean of the LI values for a given brain region r.
2. Each marginal hypothesis H_{0r} is tested by:

   a) Computing the t-statistic for the original LI values of the region r (i.e., to compute the t value corresponding to the hypothesis that the data in the vector LI come from a distribution with mean zero).
   b) Obtaining a larger number of permutation resample from the data (without replacement) and constructing the permutation distribution of the t-statistic (in each permutation the sign of at least one of the elements of the original LI vector was changed, being the complete permutation space 2^n, where n is the number of fiber tracking algorithms used).
   c) Finding the P value of H_{0r} by comparing the original t-statistic (obtained in step a) with the t-statistic permutation distribution (obtained in step b), specifically, to perform a 2-sided test (sign test) with the hypothesis that the data in the t-statistic permutation distribution come from a distribution whose median is the original t-statistic.

References

Alemán-Gómez Y, Melie-García L, Valdes-Hernández P. 2006. IBASPM: toolbox for automatic parcellation of brain structures. Neuroimage. 31(1):29–185.

Amunts K, Schlaug G, Schleicher A, Steinmetz H, Dabringhaus A, Roland PE, Zilles K. 1996. Asymmetry in the human motor cortex and handedness. Neuroimage. 4:216–222.

Amunts K, Schleicher A, Burgel U, Mohlberg H, Uylings HBM, Zilles K. 1999. Broca's region revisited: cytoarchitecture and intersubject variability. J Comp Neurol. 412:319–341.

Amunts K, Weiss PH, Mohlberg H, Pieperhoff P, Eickhoff S, Gurd JM, Marshall JC, Shah NJ, Fink GR, Zilles K. 2004. Analysis of neural mechanisms underlying verbal fluency in cytoarchitectonically defined stereotaxic space—the roles of Brodmann areas 44 and 45. Neuroimage. 22:42–56.

Aylward EH, Reiss AL, Reader MJ, Singer HS, Brown JE, Denckla MB. 1996. Basal ganglia volumes in children with attention-deficit hyperactivity disorder. J Child Neurol. 11:112–115.

Barrick TR, Mackay CE, Prima S, Maes F, Vandermeulen D, Crow TJ, Roberts N. 2005. Automatic analysis of cerebral asymmetry: an exploratory study of the relationship between brain torque and planum temporale asymmetry. Neuroimage. 24:678–691.

Basser PJ, Pajevic S, Pierpaoli C, Duda J, Aldroubi A. 2000. In vivo fiber tractography using DT-MRI data. Magn Reson Med. 44:625–632.

Bassett DS, Bullmore E, Verchinski BA, Mattay VS, Weinberger DR, Meyer-Lindenberg A. 2008. Hierarchical organization of human cortical networks in health and schizophrenia. J Neurosci. 28:9239–9248.

Bassett DS, Meyer-Lindenberg A, Achard S, Duke T, Bullmore E. 2006. Adaptive reconfiguration of fractal small-world human brain functional networks. Proc Natl Acad Sci U S A. 103:19518–19523.

Behrens TE, Johansen-Berg H, Woolrich MW, Smith SM, Wheeler-Kingshott CA, Boulby PA, Barker GJ, Sillery EL, Sheehan K, Ciccarelli O, et al. 2003. Non-invasive mapping of connections between human thalamus and cortex using diffusion imaging. Nat Neurosci. 6:750–757.

Behrens TE, Woolrich MW, Jenkinson M, Johansen-Berg H, Nunes RG, Clare S, Matthews PM, Brady JM, Smith SM. 2003. Characterization and propagation of uncertainty in diffusion-weighted MR imaging. Magn Reson Med. 50:1077–1088.

Bigler ED, Blatter DD, Anderson CV, Johnson SC, Gale SD, Hopkins RO, Burnett B. 1997. Hippocampal volume in normal aging and traumatic brain injury. Am J Neuroradiol. 18:11–23.

Bilir E, Craven W, Hugg J, Gilliam F, Martin R, Faught E, Kuzniecky R. 1998. Volumetric MRI of the limbic system: anatomic determinants. Neuroradiology. 40:138–144.

Blair RC, Karniski W. 1993. An alternative method for significance testing of wave-form difference potentials. Psychophysiology. 30:518–524.

Boccaletti S, Latora V, Moreno Y, Chavez M, Hwang D-U. 2006. Complex networks: structure and dynamics. Phys Rep. 424:175–308.

Castellanos FX, Giedd JN, Berquin PC, Walter JM, Sharp W, Tran T, Vaituzis AC, Blumenthal JD, Nelson J, Bastain TM, et al. 2001. Quantitative brain magnetic resonance imaging in girls with attention-deficit/hyperactivity disorder. Arch Gen Psychiatry. 58:289–295.

Chen ZJ, He Y, Rosa P, Germann J, Evans AC. 2008. Revealing modular architecture of human brain structural networks by using cortical thickness from MRI. Cereb Cortex. 18:2374–2381.

Clark C, Ulmer J, Gaggle W, Mark L. 2007. Structural asymmetries of the normal human cingulum. Available at http://www.marquette.edu/engineering/pages/AllYouNeed/Biomedical/Programs/documents/codi_final.pdf. Accessed 1 April 2010.

Conturo TE, Lori NF, Cull TS, Akbudak E, Snyder AZ, Shimony JS, McKinstry RC, Burton H, Raichle ME. 1999. Tracking neuronal fiber pathways in the living human brain. Proc Natl Acad Sci U S A. 96:10422–10427.

Corbetta M, Shulman GL. 2002. Control of goal-directed and stimulus-driven attention in the brain. Nat Rev Neurosci. 3:201–215.

Costa Lda F. 2005. Morphological complex networks: can individual morphology determine the general connectivity and dynamics of networks? Presented at the COSIN final meeting, Salou, Spain, March. arXiv:q-bio/0503041v1 [q-bio.MN]. Available at http://arxiv.org/abs/q-bio/0503041. Accessed 1 April 2010.

Costa Lda F, Rodrigues FA, Travieso G, Villas PR. 2007. Characterization of complex networks: A survey of measurements. Adv. Phys. 56(1):167–242.
Costa Lda F, Sporns O. 2005. Hierarchical features of large-scale cortical connectivity. Eur Phys J B. 48:567–573.
Dadda M, Cantalupo C, Hopkins WD. 2006. Further evidence of an association between handedness and neuroanatomical asymmetries in the primary motor cortex of chimpanzees (Pan troglodytes). Neuropsychologia. 44:2582–2586.
Dall'Asta L, Barrat A, Barthelemy M, Vespignani A. 2006. Vulnerability of weighted networks. J Stat Mech. Published online April 27, doi: 10.1088/1742-5468/2006/04/P04006.
Embleton KV, Lambon Ralph MA, Parker GJ. 2006. A combined distortion corrected protocol for diffusion weighted tractography and fMRI. ISMRM 14th Scientific Meeting & Exhibition; 2006 May 6–12; Seattle, WA. Vol. 14, 1070 p.
Fawcett T. 2006. An introduction to ROC analysis. Pattern Recog Lett. 27:861–874.
Filipek PA, Semrud-Clikeman M, Steingard RJ, Renshaw PF, Kennedy DN, Biederman J. 1997. Volumetric MRI analysis comparing subjects having attention-deficit hyperactivity disorder with normal controls. Neurology. 48:589–601.
Fink GR, Marshall JC, Shah NJ, Weiss PH, Halligan PW, Grosse-Ruyken M, Ziemons K, Zilles K, Freund HJ. 2000. Line bisection judgments implicate right parietal cortex and cerebellum as assessed by fMRI. Neurology. 54:1324–1331.
Fink GR, Marshall JC, Weiss PH, Zilles K. 2001. The neural basis of vertical and horizontal line bisection judgments: an fMRI study of normal volunteers. Neuroimage. 14:S59–S67.
Free SL, Bergin PS, Fish DR, Cook MJ, Shorvon SD, Stevens JM. 1995. Methods for normalization of hippocampal volumes measured with MR. Am J Neuroradiol. 16:637–643.
Freeman L. 1977. A set of measures of centrality based upon betweenness. Sociometry. 40:35–41.
Galan L, Biscay R, Rodriguez JL, PerezAbalo MC, Rodriguez R. 1997. Testing topographic differences between event related brain potentials by using non-parametric combinations of permutation tests. Electroencephalogr Clin Neurophysiol. 102:240–247.
Gannon PJ, Kheck N, Hof PR. 2008. Leftward interhemispheric asymmetry of macaque monkey temporal lobe language area homolog is evident at the cytoarchitectural, but not gross anatomic level. Brain Res. 1199:62–73.
Gil-Da-Costa R, Braun A, Lopes M, Hauser MD, Carson RE, Herscovitch P, Martin A. 2004. Toward an evolutionary perspective on conceptual representation: species-specific calls activate visual and affective processing systems in the macaque. Proc Natl Acad Sci U S A. 101:17516–17521.
Glasser MF, Rilling JK. 2008. DTI tractography of the human brain's language pathways. Cereb Cortex. 18:2471–2482.
Gong GL, He Y, Concha L, Lebel C, Gross DW, Evans AC, Beaulieu C. 2009. Mapping anatomical connectivity patterns of human cerebral cortex using in vivo diffusion tensor imaging tractography. Cereb Cortex. 19:524–536.
Gong GL, Jiang TZ, Zhu CZ, Zang YF, Wang F, Xie S, Xiao JX, Gu XM. 2005. Asymmetry analysis of cingulum based on scale-invariant parameterization by diffusion tensor imaging. Hum Brain Mapp. 24:92–98.
Good CD, Johnsrude I, Ashburner J, Henson RNA, Friston KJ, Frackowiak RSJ. 2001a. Cerebral asymmetry and the effects of sex and handedness on brain structure: a voxel-based morphometric analysis of 465 normal adult human brains. Neuroimage. 14:685–700.
Good CD, Johnsrude IS, Ashburner J, Henson RNA, Friston KJ, Frackowiak RSJ. 2001b. A voxel-based morphometric study of ageing in 465 normal adult human brains. Neuroimage. 14:21–36.
Graybiel AM. 2005. The basal ganglia: learning new tricks and loving it. Curr Opin Neurobiol. 15:638–644.
Hagmann P, Cammoun L, Gigandet X, Meuli R, Honey CJ, Wedeen V, Sporns O. 2008. Mapping the structural core of human cerebral cortex. PLoS Biol. 6:1479–1493.
Hagmann P, Cammoun L, Martuzzi R, Maeder P, Clarke S, Thiran JP, Meuli R. 2006. Hand preference and sex shape the architecture of language networks. Hum Brain Mapp. 27:828–835.
Hagmann P, Kurant M, Gigandet X, Thiran P, Wedeen VJ, Meuli R, Thiran JP. 2006. Imaging the brain neuronal network with diffusion MRI: a way to understand its global architecture. ISMRM 14th Scientific Meeting & Exhibition; 2006 May 6–12; Seattle, WA. Vol. 14, 436 p.
Halligan PW, Fink GR, Marshall JC, Vallar G. 2003. Spatial cognition: evidence from visual neglect. Trends Cogn Sci. 7:125–133.
Haroon HA, Morris DM, Embleton KV, Alexander DC, Parker GJM. 2009. Using the model-based residual bootstrap to quantify uncertainty in fiber orientations from Q-ball analysis. IEEE Trans Med Imaging. 28:535–550.
Haroon HA, Morris DM, Kaiser A, Augath M, Logothetis NK, Parker GJ. 2008. Comparing corticocortical interconnection information from tracer studies and probabilistic tractography in the postmortem macaque brain. ISMRM 16th Scientific Meeting & Exhibition; 2008 May 3–9; Toronto, Ontario, Canada, p. 3369.
He Y, Chen ZJ, Evans AC. 2007. Small-world anatomical networks in the human brain revealed by cortical thickness from MRI. Cereb Cortex. 17:2407–2419.
He Y, Chen Z, Evans AC. 2008. Structural insights into aberrant topological patterns of large-scale cortical networks in Alzheimer's disease. J Neurosci. 28:4756–4766.
Heffner HE, Heffner RS. 1984. Temporal lobe lesions and perception of species-specific vocalizations by macaques. Science. 226: 75–76.
Honey CJ, Kotter R, Breakspear M, Sporns O. 2007. Network structure of cerebral cortex shapes functional connectivity on multiple time scales. Proc Natl Acad Sci U S A. 104:10240–10245.
Husain M, Rorden C. 2003. Non-spatially lateralized mechanisms in hemispatial neglect. Nat Rev Neurosci. 4:26–36.
Iturria-Medina Y, Canales-Rodríguez EJ, Melie-García L, Valdes-Hernández PA, Martínez-Montes E, Alemán-Gómez Y, Sánchez-Bornot JM. 2007. Characterizing brain anatomical connections using diffusion weighted MRI and graph theory. Neuroimage. 36:645–660.
Iturria-Medina Y, Sotero RC, Canales-Rodriguez EJ, Alemán-Gómez Y, Melie-Garcia L. 2008. Studying the human brain anatomical network via diffusion-weighted MRI and Graph Theory. Neuroimage. 40:1064–1076.
Juch H, Zimine I, Seghier ML, Lazeyras F, Fasel JHD. 2005. Anatomical variability of the lateral frontal lobe surface: implication for intersubject variability in language neuroimaging. Neuroimage. 24:504–514.
Keller SS, Crow T, Foundas A, Amunts K, Roberts N. 2009. Broca's area: nomenclature, anatomy, typology and asymmetry. Brain Lang. 109:29–48.
Koch MA, Norris DG, Hund-Georgiadis M. 2002. An investigation of functional and anatomical connectivity using magnetic resonance imaging. Neuroimage. 16:241–250.
Kubicki M, Westin CF, Maier SE, Frumin M, Nestor PG, Salisbury DF, Kikinis R, Jolesz FA, McCarley RW, Shenton ME. 2002. Uncinate fasciculus findings in schizophrenia: a magnetic resonance diffusion tensor imaging study. Am J Psychiatry. 159: 813–820.
Latora V, Marchiori M. 2001. Efficient behavior of small-world networks. Phys Rev Lett. 87:198701.
Lerch JP, Worsley K, Shaw WP, Greenstein DK, Lenroot RK, Giedd J, Evans AC. 2006. Mapping anatomical correlations across cerebral cortex (MACACC) using cortical thickness from MRI. Neuroimage. 31:993–1003.
Lewis JW, Van Essen DC. 2000. Mapping of architectonic subdivisions in the macaque monkey, with emphasis on parieto-occipital cortex. J Comp Neurol. 428:79–111.
Li YH, Liu Y, Li J, Qin W, Li KC, Yu CS, Jiang TZ. 2009. Brain anatomical network and intelligence. PLoS Comput Biol. 5:e1000395.
Lindenberg R, Fangerau H, Seitz RJ. 2007. "Broca's area" as a collective term? Brain Lang. 102:22–29.
Luders E, Narr KL, Thompson PM, Rex DE, Jancke L, Toga AW. 2006. Hemispheric asymmetries in cortical thickness. Cereb Cortex. 16:1232–1238.

Mazziotta J, Toga A, Evans A, Fox P, Lancaster J, Zilles K, Woods R, Paus T, Simpson G, Pike B, et al. 2001. A four-dimensional probabilistic atlas of the human brain. J Am Med Inform Assoc. 8:401–430.
Mazziotta JC, Toga AW, Evans A, Fox P, Lancaster J. 1995. A probabilistic atlas of the human brain: theory and rationale for its development. The International Consortium for Brain Mapping (ICBM). Neuroimage. 2:89–101.
Mori S, Crain BJ, Chacko VP, van Zijl PC. 1999. Three-dimensional tracking of axonal projections in the brain by magnetic resonance imaging. Ann Neurol. 45:265–269.
Morris DM, Embleton KV, Parker GJM. 2008. Probabilistic fibre tracking: differentiation of connections from chance events. Neuroimage. 42:1329–1339.
Niznikiewicz M, Donnino R, McCarley RW, Nestor PG, Iosifescu DV, O'Donnell B, Levitt J, Shenton ME. 2000. Abnormal angular gyrus asymmetry in schizophrenia. Am J Psychiatry. 157: 428–437.
Onnela JP, Saramaki J, Kertesz J, Kaski K. 2005. Intensity and coherence of motifs in weighted complex networks. Phys Rev E. 71:065103.
Packard MG, Knowlton BJ. 2002. Learning and memory functions of the basal ganglia. Annu Rev Neurosci. 25:563–593.
Parker GJM, Alexander DC. 2005. A mechanism for probabilistic fibre tracking using multi-fibre orientation functions. ISMRM Workshop on Methods for Quantitative Diffusion MRI of the brain; 2005 March 13–16; Lake Louise, Alberta, Canada. 74 p.
Parker GJM, Haroon HA, Wheeler-Kingshott CA. 2003. A framework for a streamline-based probabilistic index of connectivity (PICo) using a structural interpretation of MRI diffusion measurements. J Magn Reson Imaging. 18:242–254.
Parker GJM, Wheeler-Kingshott CA, Barker GJ. 2002. Estimating distributed anatomical connectivity using fast marching methods and diffusion tensor imaging. IEEE Trans Med Imaging. 21:505–512.
Parker GJM, Luzzi S, Alexander DC, Wheeler-Kingshott CAM, Clecarelli O, Ralph MAL. 2005. Lateralization of ventral and dorsal auditory-language pathways in the human brain. Neuroimage. 24: 656–666.
Paus T, Otaky N, Caramanos Z, MacDonald D, Zijdenbos A, DAvirro D, Gutmans D, Holmes C, Tomaiuolo F, Evans AC. 1996. In vivo morphometry of the intrasulcal gray matter in the human cingulate, paracingulate, and superior-rostral sulci: hemispheric asymmetries, gender differences and probability maps. J Comp Neurol. 376:664–673.
Pegues MP, Rogers LJ, Amend D, Vinogradov S, Deicken RF. 2003. Anterior hippocampal volume reduction in male patients with schizophrenia. Schizophr Res. 60:105–115.
Poremba A, Malloy M, Saunders RC, Carson RE, Herscovitch P, Mishkin M. 2004. Species-specific calls evoke asymmetric activity in the monkey's temporal poles. Nature. 427:448–451.
Powell HWR, Parker GJM, Alexander DC, Symms MR, Boulby PA, Wheeler-Kingshott CAM, Barker GJ, Noppeney U, Koepp MJ, Duncan JS. 2006. Hemispheric asymmetries in language-related pathways: a combined functional MPI and tractography study. Neuroimage. 32:388–399.
Price CJ. 2000. The anatomy of language: contributions from functional neuroimaging. J Anat. 197:335–359.
Pueyo R, Maneru C, Vendrell P, Mataro N, Estevez-Gonzalez A, Garcia-Sanchez C, Junque C. 2000. Attention deficit hyperactivity disorder. Cerebral asymmetry observed on magnetic resonance. Rev Neurol. 30:920–925.
Rodrigo S, Naggara O, Oppenheirn C, Golestani N, Poupon C, Cointepas Y, Mangin JF, Le Bihan D, Meder JF. 2007. Human subinsular asymmetry studied by diffusion tensor Imaging and fiber tracking. Am J Neuroradiol. 28:1526–1531.
Rogers BP, Carew JD, Meyerand ME. 2004. Hemispheric asymmetry in supplementary motor area connectivity during unilateral finger movements. Neuroimage. 22:855–859.
Schrimsher GW, Billingsley RL, Jackson EF, Moore BD. 2002. Caudate nucleus volume asymmetry predicts attention-deficit hyperactivity disorder (ADHD) symptomatology in children. J Child Neurol. 17:877–884.
Sporns O. 2006. Small-world connectivity, motif composition, and complexity of fractal neuronal connections. Biosystems. 85:55–64.
Sporns O, Zwi JD. 2004. The small world of the cerebral cortex. Neuroinformatics. 2:145–162.
Sugama S, Bingham PM, Wang PP, Moss EM, Kobayashi H, Eto Y. 2000. Morphometry of the head of the caudate nucleus in patients with velocardiofacial syndrome (del 22q11.2). Acta Paediatr. 89:546–549.
Toga A, Thompson P, Susumu M, Amunts K, Zilles K. 2006. Towards multimodal atlases of the human brain. Nat Rev Neurosci. 7(12):952–966.
Tremols V, Bielsa A, Soliva JC, Raheb C, Carmona S, Tomas J, Gispert JD, Rovira M, Fauquet J, Tobena A, et al. 2008. Differential abnormalities of the head and body of the caudate nucleus in attention deficit-hyperactivity disorder. Psychiat Res Neuroimaging. 163:270–278.
Tuch DS. 2004. Q-ball imaging. Magn Reson Med. 52:1358–1372.
Tuch DS, Reese TG, Wiegell MR, Wedeen VJ. 2003. Diffusion MRI of complex neural architecture. Neuron. 40:885–895.
Vallar G. 1998. Spatial hemineglect in humans. Trends Cogn Sci. 2:87–97.
Van Essen DC. 1997. A tension-based theory of morphogenesis and compact wiring in the central nervous system. Nature. 385:313–318.
Wang JH, Wang L, Zang YF, Yang H, Tang HH, Gong QY, Chen Z, Zhu CZ, He Y. 2009. Parcellation-dependent small-world brain functional networks: a resting-state fMRI study. Hum Brain Mapp. 30:1511–1523.
Watkins KE, Paus T, Lerch JP, Zijdenbos A, Collins DL, Neelin P, Taylor J, Worsley KJ, Evans AC. 2001. Structural asymmetries in the human brain: a voxel-based statistical analysis of 142 MRI scans. Cereb Cortex. 11:868–877.
Watts DJ, Strogatz SH. 1998. Collective dynamics of small-world networks. Nature. 393(6684):440–442.